JOURNAL OF SPACECRAFT AND ROCKETS
Vol. 29, No. 5, September-October 1992

Numerical Dissipation in F3D Thin-Layer Navier-Stokes Solution for Flows with Wall Transpiration

M. Kandula*
Lockheed Engineering & Sciences Company, Houston, Texas 77058
and
F. W. Martin Jr.†
NASA Johnson Space Center, Houston, Texas 77058

Numerical boundary conditions for mass injection/suction at the wall are incorporated in the thin-layer Navier-Stokes code, F3D. The accuracy of the boundary conditions and the code is assessed by a detailed comparison of the predictions of velocity distributions and skin-friction coefficients with exact similarity solutions for laminar flow over a flat plate with variable blowing/suction, and measurements for turbulent flow past a flat plate with uniform blowing. In laminar flow, F3D predictions for friction coefficient compare well with exact similarity solution with and without suction, but the code produces large errors at moderate-to-large values of blowing. These errors are attributed to the numerical dissipation due to Steger-Warming flux-vector splitting in the upwinding (streamwise) direction. This numerical dissipation is shown to yield a slight Mach number dependence of skin-friction coefficient due to blowing in turbulent flow. Predicted surface pressures for turbulent flow past an airfoil with mass injection are in qualitative agreement with measurements for a flat plate.

Nomenclature

A,B,C,M	= flux Jacobians
a	= velocity of sound
C	= blowing parameter for similarity in laminar flow
c_{fx}	= local skin-friction coefficient
D_e,D_i	= explicit and implicit dissipation parameters
$D_{n,\xi},D_{n,\zeta}$	= numerical dissipation due to flux-vector splitting in ξ and ζ directions
d	= normal distance from the wall
e	= total energy per unit volume
F	$= \rho_w w_b/(\rho_\infty u_\infty)$
F,G,H	= inviscid flux vectors in ξ, η, and ζ directions
f	= stretching parameter
h	= Δt or $\Delta t/2$ for first- or second-order time accuracy
i,j,k	= grid indices in ξ, η, and ζ directions, respectively
J	= Jacobian of transformation
K	= mixing length constant
L	= reference length
ℓ	= mixing length
M	= Mach number
Pr	= Prandtl number
p	= static pressure
Q	= vector of conservative flow variables
R	= gas constant
Re	= Reynolds number
S	= viscous flux vector
T	= temperature
t	= time
U,V,W	= contravariant velocities
u^*	= friction velocity
u_∞	= freestream velocity
u,v,w	= Cartesian velocity components in x, y, and z, directions, respectively
w_b	= blowing velocity normal to the wall
x,y,z	= Cartesian coordinate directions
α	= dissipation coefficient
β	= smoothing coefficient for the boundary layer
Δt	= time increment
$\Delta x, \Delta z$	= local grid spacings in x and z directions
δ	= three-point central difference operator
$\delta_\xi^b,\delta_\xi^f$	= backward and forward difference operators
$\bar{\delta}$	= midpoint operator
γ	= specific heat ratio
ϵ	= smoothing parameter for artificial dissipation
ϵ_i	= eddy viscosity in inner region
η	= similarity variable, $z\sqrt{u_\infty/\nu x}$
μ	= dynamic viscosity
ν	= kinematic viscosity
ξ,η,ζ	= transformed coordinates
ρ	= density
σ	= modified spectral radius of C
τ_w	= wall shear stress
ω	= local vorticity

Subscripts

b	= blowing/suction
w	= wall
x	= local (streamwise)
∞	= freestream

Superscript

	= dimensional quantities

Presented as Paper 91-3204 at the AIAA 9th Applied Aerodynamics Conference, Baltimore, MD, Sept. 23-25, 1991; received Oct. 4, 1991; revision received Feb. 18, 1992; accepted for publication Feb. 21, 1992.

*Advanced Systems Engineering Specialist. Senior Member AIAA.
†Group Leader. Member AIAA.

Introduction

SECONDARY flow from surfaces arises in numerous applications, such as thermal protection systems (transpiration, film, and ablation cooling), boundary-layer control (lift increase or drag reduction), thrust vector control, and surface venting. The degree of interaction between the secondary flow

and the main flow depends on a wall-blowing parameter $F = \rho_w w_b/(\rho_\infty u_\infty)$. At large values of F, the flowfield is altered significantly, resulting in large changes in surface pressure, friction, and heat transfer.

To numerically simulate such physical processes, the boundary conditions of mass injection/suction and heat transfer at the surface are incorporated into the widely used three-dimensional, thin-layer, compressible Navier-Stokes code, F3D, developed by NASA Ames.[1] This code is used to simulate the Space Shuttle aerodynamic flowfield.[2] The simulation of venting from various surfaces such as the wing leading edge of the Shuttle Orbiter has motivated the present investigation.

In a recent paper, Roth[3] has applied the F3D code to study the influence of thin-layer approximation on the three-dimensional structure of a subsonic round jet issuing normally through a flat plate into a crossflow. The maximum velocity ratio considered is 6. Only laminar flow is considered. The effect of thin-layer approximation in both one and two directions is evaluated. The present paper focuses on the validation of the code for two-dimensional flow with blowing/suction at the surface, in both laminar and turbulent flow.

Numerical Algorithm

The accuracy of the F3D code is tested against available exact solutions for steady, two-dimensional laminar flow and measurements for turbulent flow past a flat plate. Additionally, numerical solutions for boundary-layer equations are obtained to provide an additional check on the accuracy of the implementation of wall boundary conditions and turbulence model. The boundary-layer solution algorithm is built into the overall F3D code. A brief description of the F3D code and the boundary-layer code is given next.

F3D Code

The compressible thin-layer Navier-Stokes code, F3D, described in Refs. 1 and 2, solves the three-dimensional, unsteady flow governing equations in conservative form in generalized coordinates (ξ, η, ζ) that are transformations of the rectangular Cartesian space (x, y, z). Thin-layer approximation is used in the ζ direction (normal to the body) in which viscous terms are retained, whereas in the ξ and η directions (parallel to the body) all viscous terms are neglected. The algorithm is based on an implicit Beam-Warming[4] type two-factor approximately factored scheme. Steger-Warming flux-vector splitting[5] and upwind differencing are considered in the streamwise direction. Central differencing is applied in the remaining spatial directions, with artificial dissipation added for maintaining stability. Numerical dissipation is inherently present in the upwind difference scheme, so that stability is ensured without an artificial dissipation needed in that direction. The differencing method is second-order accurate in both space and time. Only a brief outline of the governing equations and the algorithm is presented here.

In the F3D code, the dimensionless variables are defined as

$$x=\frac{x'}{L'},\quad y=\frac{y'}{L'},\quad z=\frac{z'}{L'},\quad t=\frac{t'u'_\infty}{L'}$$

$$\rho=\frac{\rho'}{\rho'_\infty},\quad u=\frac{u'}{a'_\infty},\quad v=\frac{v'}{a'_\infty},\quad w=\frac{w'}{a'_\infty},\quad p=\frac{p'}{\rho'_\infty a'^2_\infty}$$

$$e=\frac{e'}{\rho'_\infty a'^2_\infty},\quad R=\frac{R'}{R'_\infty}$$

$$T=\frac{p}{\rho R}=\frac{T'}{T'_\infty \gamma'},\quad \mu=\frac{\mu'}{\mu'_\infty}$$

$$R_{e_a}=\frac{\rho'_\infty a'_\infty L}{M'_\infty},\quad Re=\frac{\rho'_\infty u'_\infty L'_\infty}{\mu'_\infty},\quad M=\frac{u'}{a'}$$

The resulting thin-layer Navier-Stokes equations written in generalized curvilinear coordinates are

$$\partial_\tau \boldsymbol{Q}+\partial_\xi \boldsymbol{F}+\partial_\eta \boldsymbol{G}+\partial_\zeta \boldsymbol{H}=Re^{-1}\partial_\zeta \boldsymbol{S} \tag{1}$$

where

$$\boldsymbol{Q}=J^{-1}\begin{bmatrix}\rho\\ \rho u\\ \rho v\\ \rho w\\ e\end{bmatrix},\qquad \boldsymbol{F}=J^{-1}\begin{bmatrix}\rho U\\ \rho uU+\xi_x p\\ \rho vU+\xi_y p\\ \rho wU+\xi_z p\\ (e+p)U-\xi_t p\end{bmatrix}$$

$$\boldsymbol{G}=J^{-1}\begin{bmatrix}\rho V\\ \rho uV+\eta_x p\\ \rho vV+\eta_y p\\ \rho wV+\eta_z p\\ (e+p)V-\eta_t p\end{bmatrix},\qquad \boldsymbol{H}=J^{-1}\begin{bmatrix}\rho W\\ \rho uW+\zeta_x p\\ \rho vW+\zeta_y p\\ \rho wW+\zeta_z p\\ (e+p)W-\zeta_t p\end{bmatrix}$$

$$\boldsymbol{S}=J^{-1}\mu\begin{bmatrix}0\\ m_1u_\zeta+(\tfrac{1}{3})m_2\zeta_x\\ m_1v_\zeta+(\tfrac{1}{3})m_2\zeta_y\\ m_1w_\zeta+(\tfrac{1}{3})m_2\zeta_z\\ m_1m_3+(\tfrac{1}{3})m_2(\zeta_x u+\zeta_y v+\zeta_z w)\end{bmatrix}$$

with the contravariant velocities

$$U=\xi_t+\xi_x u+\xi_y v+\xi_z w$$

$$V=\eta_t+\eta_x u+\eta_y v+\eta_z w$$

$$W=\zeta_t+\zeta_x u+\zeta_y v+\zeta_z w$$

and

$$m_1=\zeta_x^2+\zeta_y^2+\zeta_z^2$$

$$m_2=\zeta_x u_\zeta+\zeta_y v_\zeta+\zeta_z w_\zeta$$

$$m_3=[(u^2+v^2+w^2)_\zeta/2]+Pr^{-1}(\gamma-1)^{-1}(a^2)_\zeta$$

where ξ_x, ξ_y, ξ_z, ξ_t, etc., denote the metrics of the transformation. Perfect gas and a constant Pr are assumed in the analysis.

The pressure is related to the conservative flow variables $\boldsymbol{Q}$ by the equation of state

$$p=(\gamma-1)[e-\tfrac{1}{2}\rho(u^2+v^2+w^2)] \tag{2}$$

The final discretized equations in F3D are of the form

$$L_1L_2\Delta\boldsymbol{Q}^{n+1}=-\Delta t\{\partial_\xi^b(\boldsymbol{F}^+)^n+\partial_\xi^f(\boldsymbol{F}^-)^n+\partial_\eta \boldsymbol{G}^n+\partial_\zeta \boldsymbol{H}^n$$
$$-Re^{-1}\bar{\delta}_\zeta \boldsymbol{S}^n\}-(D_e|_\eta+D_e|_\zeta)\boldsymbol{Q}^n \tag{3}$$

where the forward and backward operators L_1 and L_2 are given by

$$L_1=I+h\delta_\xi^b(\boldsymbol{A}^+)^n+h\delta_\zeta \boldsymbol{C}^n-hRe^{-1}\bar{\delta}_\zeta J^{-1}\boldsymbol{M}^n J-D_i|_\zeta$$

$$L_2=I+h\delta_\xi^f(\boldsymbol{A}^-)^n+h\delta_\eta \boldsymbol{B}^n-D_i|_\eta$$

The flux $\boldsymbol{F}$ in the ξ direction is eigensplit into $\boldsymbol{F}^+$ and $\boldsymbol{F}^-$, which are then differenced with the use of backward and forward difference operators δ_ξ^b and δ_ξ^f, which can be of second order (three point) or first order (two point). The 5×5 ma-

trices A, B, C, and M result from local linearization of the fluxes F, G, H, and S about the previous time level n. The quantities D_i and D_e are the implicit and explicit dissipation operators in the central space differencing directions η and ζ, to suppress high frequency oscillations. The explicit artificial dissipation operator, which influences the accuracy of the steady-state solution, for example in the z direction, is of the form

$$D_e|_\zeta = (\Delta t)J^{-1}\epsilon\left\{\bar{\delta}\sigma\alpha\bar{\delta} + \bar{\delta}\frac{\sigma}{1+\alpha}\bar{\delta}^3\right\}\Big|_\zeta J \tag{4a}$$

where α is a dissipation coefficient proportional to the absolute value of a normalized second difference of pressure, expressed as

$$\alpha = \left(\frac{1+M_\infty^\gamma}{16}\right)\frac{|\bar{\delta}^2 p|}{|(1+\bar{\delta}^2)p|} \tag{4b}$$

and σ is a modified spectral radius of C given by

$$\sigma|U| + \sqrt{(\zeta_x^2+\zeta_y^2+\zeta_z^2)\bar{c}^2 + 0.01} \tag{4c}$$

$$\bar{c}^2 = \frac{\gamma p}{\rho}(1-\beta) + \frac{\beta(u^2+v^2+w^2)}{M_\infty^2} \tag{4d}$$

The second-order smoothing controls numerical oscillations in regions with steep gradients (large α) such as shocks, and the fourth-order smoothing is effective elsewhere. A value of $\beta = 1$ reduces the numerical smoothing in the boundary layer near the surface. Second-order upwinding is considered in all of the present calculations.

Boundary-Layer Code

The boundary-layer code solves the three-dimensional, unsteady flow boundary-layer equations in conservative form in generalized coordinates (ξ, η, ζ). The solution is iterated over time. During each time step, a solution is obtained by marching along the ξ direction. At each $\xi = \text{const}$ station, the momentum and energy in the (η-ζ) plane are solved for using an implicit method involving the inversion of tridiagonal matrices. The solution is then corrected by the application of the continuity equation. The method is second-order accurate in space and time.

Boundary Conditions

Wall Boundaries

Necessary modifications to the F3D code are made to include the boundary condition for wall blowing/suction. The contravariant velocities U and V tangential to the surface are taken as zero to satisfy the no-slip condition at the wall, and the contravariant velocity W normal to the surface is specified. Zero normal pressure gradient at the wall is considered to specify the surface pressure p_w. Mathematically,

$$U = 0, \qquad V = 0 \tag{5a}$$

$$W = \sqrt{(\zeta_x^2+\zeta_y^2+\zeta_z^2)}M_\infty F(\rho_\infty/\rho_w) \tag{5b}$$

$$\frac{\partial p}{\partial z} = 0 \tag{5c}$$

where

$$F = \rho_w w_b/(\rho_\infty u_\infty)$$

For the case of adiabatic wall, the density at the wall ρ_w is obtained by extrapolation in the normal direction, and the wall temperature is computed from the equation of state. In the case of wall heat transfer, the wall temperature T_w is specified, and the density at the wall is computed from the equation of state, knowing the surface pressure and surface temperature. The total energy per unit volume e_w is computed from the known p_w and ρ_w.

Inflow, Outflow, and Free Boundaries

Freestream conditions are specified at the inflow boundary. The top (free) boundary and the outflow variables are obtained from the interior solution by linear extrapolation. All boundary conditions are applied explicitly.

Turbulence Model

The turbulence model is also modified to reflect the changes in turbulence structure due to blowing. In the existing Baldwin-Lomax model,[6] the Van Driest damping constant is expressed as a function of the blowing velocity to freestream velocity ratio, in accordance with Cebeci-Smith model.[7]

The eddy viscosity in the inner region ϵ_1 is computed from

$$\epsilon_i = \ell^2|\omega| \tag{6a}$$

where $|\omega|$ is the absolute magnitude of local vorticity, and the mixing length ℓ is described by

$$\ell = Kd[1 - \exp(-d^+/A^+)] \tag{6b}$$

where

$$d^+ = \rho_w u^* d/\mu_w = d\sqrt{\rho_w \tau_w}/\mu_w \tag{6c}$$

$$A^+ = 26\exp[5.9(\mu_w/\mu)w_b^+] \tag{6d}$$

$$w_b^+ = w_b/u^* = F(\rho_\infty/\rho_w)(u_\infty/u^*) \tag{6e}$$

$$u^* = \sqrt{\tau_w/\rho_w} \tag{6f}$$

where $K = 0.4$.

Results and Discussion

All of the calculations are made for steady-state conditions. Local time stepping is thus employed to accelerate convergence. A value of $Pr = 0.72$ is considered.

Two-Dimensional Flat Plate

The accuracy of the numerical boundary conditions incorporated in the thin-layer Navier-Stokes code is tested in laminar and turbulent flow past an adiabatic flat plate over a wide range of Reynolds number Re from 5×10^3 to 10^8 and a freestream Mach number from 0.2 to 2.0. The reference length L' is taken as 1.0 m.

Experience has shown that, in the case of blowing, numerical instability sets in if the blowing boundary condition is applied right from the leading edge. The problem is overcome by implementing the blowing condition from the third grid point in the streamwise direction.

Laminar Flow

In laminar flow, the computational fluid dynamics results at $Re = 2\times10^4$ and $M_\infty = 0.5$ are checked with exact similarity solutions[8] for incompressible boundary layers with constant properties. The solution is presented as

$$u/u_\infty = f(\eta, C) \tag{7}$$

where $C = 2F\sqrt{Re_x}$ and x is the distance from the leading edge.

Thus, by keeping a constant value of C, nonuniform blowing along the wall is maintained to insure similarity. Positive values of F or C represent blowing of fluid into the main flow, and negative values indicate suction from the main flow. In the case of blowing, the secondary fluid is assumed to be the same as the main fluid. For purposes of comparison, solutions from a boundary-layer version of the code (based on space marching) are also generated.

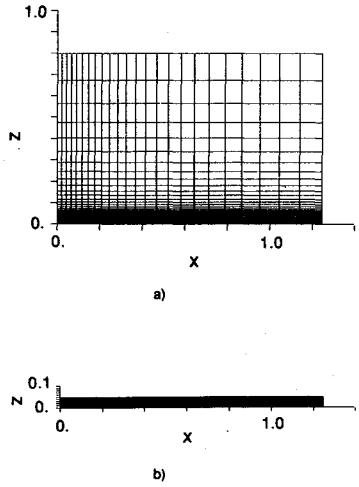

Fig. 1 Typical grids for flat plate calculation: a) 25×3×61 grid for the F3D solution, and b) 25×3×41 grid for boundary-layer solution.

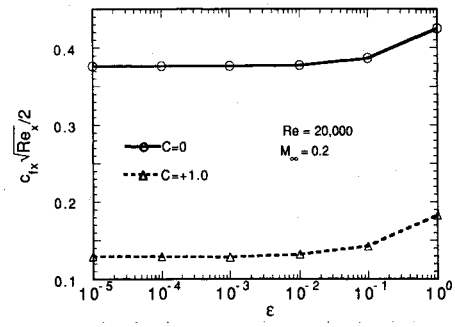

Fig. 2 Effect of artificial smoothing parameter on F3D solution for laminar flow past a flat plate at $Re = 2\times10^4$.

Figures 1a and 1b show typical grids for use in Navier-Stokes solution (25×3×61 grid) and boundary-layer solution (25×3×41 grid), respectively. The plate length (x direction) and width (symmetric y direction) are taken as 1.25 and 2.0, respectively. The grid is clustered in the x direction, with the second grid point at a distance of 0.02 from the leading edge and a stretching factor $f = 1.075$. The stretching factor f is defined as the ratio of two consecutive spacings and becomes $\Delta x_i/\Delta x_{i-1}$ for the x direction, and $\Delta x_j/\Delta x_{j-1}$ for the z direction.

For the Navier-Stokes solution, the grid is exponentially clustered in the normal direction up to $z = 0.05$ with 41 cells, resulting in a variable stretching (maximum of 1.16 at the first cell and 1.01 for the 41st cell). Beyond $z = 0.05$, the grid is stretched at a constant ratio of 1.2, resulting in $z_{max} = 0.8$. The second grid point is at a distance of 0.00007 from the wall. The artificial smoothing parameter ϵ (in the central differencing direction) in Eq. (4a) is decreased from 0.15 to 0.001. Figure 2 displays the dependence of $c_{fx}\sqrt{Re_x}/2$ with ϵ for $C = 0$ and $+1.0$. The solution (taken at $x = 0.645$) becomes independent of ϵ for ϵ less than about 0.001. Thus a value of $\epsilon = 0.001$ is considered adequate in the present work. The value of $\beta = 1.0$ in Eq. (4d) is found to yield a more accurate result than with $\beta = 0$, so that $\beta = 1.0$ is used in the present study. The solution converges in about 500 iterations.

The value of z_{max} is taken to be 0.1 for the boundary-layer code, with exponential clustering, with the second grid point at a distance of 0.000141 away from the wall. This value for z_{max} is based on a boundary-layer thickness of 0.035 at $Re = 2\times10^4$. The boundary-layer solution converges fast in less than 50 iterations.

To test the similarity law, Fig. 3 displays the velocity distributions from the F3D solution at several streamwise positions. Similarity is seen to be preserved for x in excess of about 0.2, for values of $C < 0.5$.

The computed velocity profiles from the Navier-Stokes solution (taken at $x = 0.645$) and the boundary-layer solution (taken at $x = 1.042$) for various values of C are compared in Fig. 4 with exact similarity solutions. At $C = 0$, the exact solution is given by the familiar Blasius profile. The results from the Navier-Stokes code exhibit velocity overshoots, which are known to be characteristic of Navier-Stokes solutions.[9] The maximum overshoot is seen to be of the order of 4%. In the case of suction, both Navier-Stokes and boundary-layer solutions agree well with the data. In the case of blowing, the Navier-Stokes solution is seen to be inaccurate even at $C = +0.5$, whereas the boundary-layer solution is accurate up to $C = +1.0$. According to the exact similarity solution, the laminar boundary layer separates at $C = 1.238$. Overall, the solution from the boundary-layer code is better than the Navier-Stokes solution for the simulation of laminar boundary layer with mass injection.

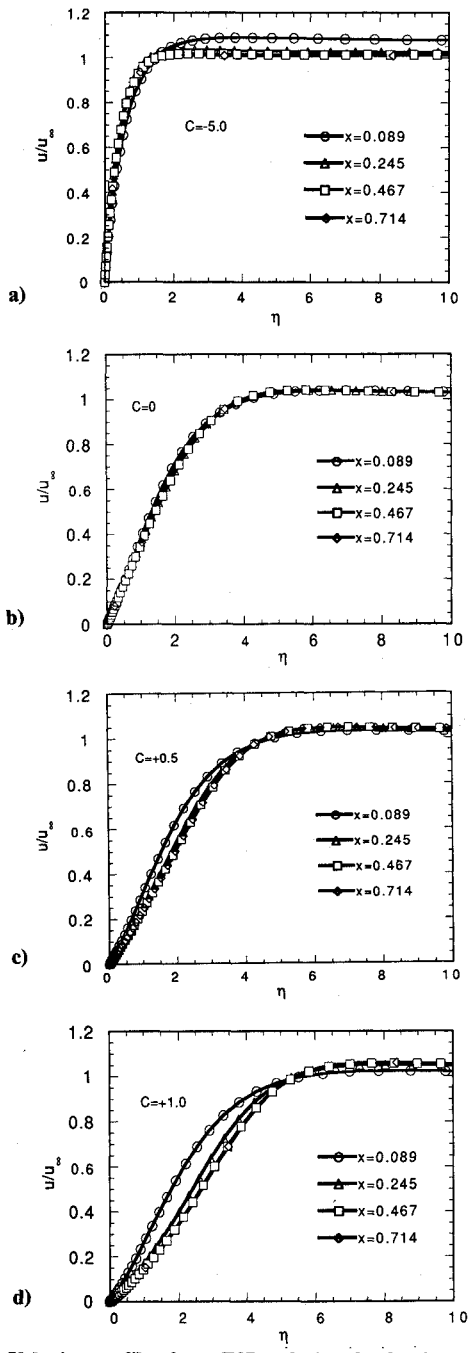

Fig. 3 Velocity profiles from F3D solution for laminar flow past a flat plate at $Re = 2\times10^4$: a) $C = -5.0$, b) $C = 0$, c) $C = +0.5$, and d) $C = +1.0$.

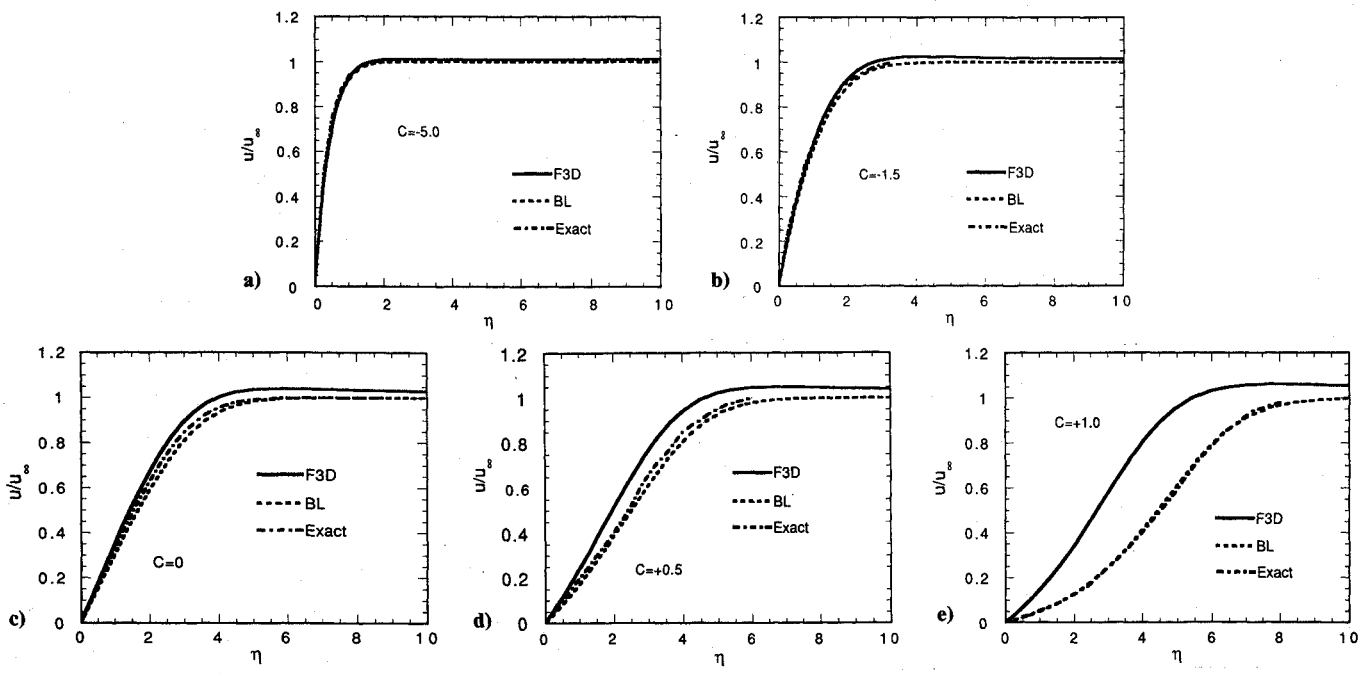

Fig. 4 Comparison of velocity profiles from F3D solution with similarity solution and boundary-layer solution for laminar flow past a flat plate with mass transfer at the wall: a) $C = -5.0$, b) $C = -1.5$, c) $C = 0$, d) $C = +0.5$, and e) $C = +1.0$.

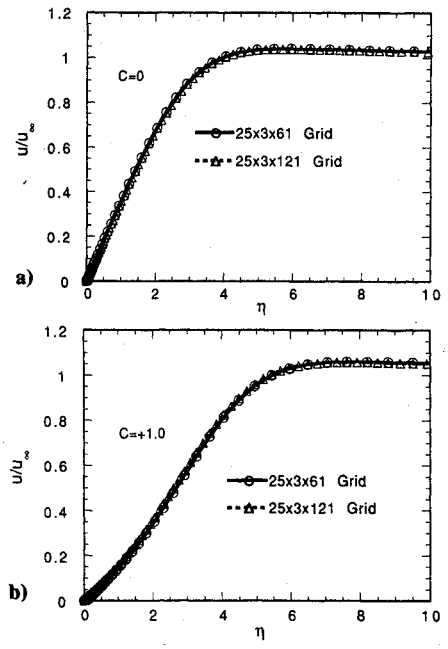

Fig. 5 Effect of grid size on F3D solution for laminar flow past a flat plate at $Re = 2 \times 10^4$; a) $C = 0$, and b) $C = +1.0$.

Grid independence of the F3D solution is examined by increasing only the resolution in the z direction, in which significant flow gradients exist. Starting with the $25 \times 3 \times 61$ grid, the z direction grid points are doubled, inserting a grid point in the middle of every grid cell of the original grid ($25 \times 3 \times 61$), so that a finer grid of $25 \times 3 \times 121$ size is generated. Figures 5a and 5b depict the velocity distributions for the two grids at $C = 0$ and $+1.0$, respectively. The solutions are seen to be very close for the two grids, both for $C = 0$ and 1.0. The friction factors differ by only about 1%. This ensures grid independence of the numerical solutions.

The study has also provided useful insight into the role of grid clustering and grid stretching in the normal direction, where severe gradients exist in the boundary layer. The rate of grid stretching in the normal direction is found to have an important effect on the velocity profiles, friction, and heat transfer. Stretching factors in excess of about 1.2 have resulted in large errors in the velocity profiles and friction coefficients. A maximum stretching factor of 1.2 is thus considered appropriate in the present work. These observations are consistent with recent findings by von Lavante[10] that, with a stretching factor of 1.3, the accuracy of the second-order van Leer's flux-vector splitting scheme is reduced to less than the first order, resulting in a diffusion of the boundary layer. The results are not quite sensitive to grid stretching in the streamwise direction for the flat plate, where streamwise gradients are small.

Table 1 compares the predicted values of $c_{fx}\sqrt{Re_x}/2$ with exact solution as a function of the parameter C. The results are also presented in Fig. 6. The data for the exact solutions are obtained from Kays.[11] Computations from F3D yield an error of 13% at $C = 0$, and the error increases with increasing C for positive values of C—40% at $C = +0.5$, and 86% at $C = +0.75$. Thus even at moderate values of blowing (say, $C = +0.5$), the error is seen to be significant. In the case of suction, however, F3D is accurate within 6%. On the other hand, the boundary-layer code results are in an error of 5% for $C \leq 0.75$ and a maximum error of 7% at $C = +1.0$.

The inadequacy of the F3D solution for laminar flow with high lateral flux for $C > 0$ is perhaps due to the observation[12] that upwinding in the flux-vector splitting schemes (Steger-Warming[5] and van Leer[13]) produces large numerical dissipation in the boundary layer, as compared to that in flux difference splitting schemes such as those of Roe[14] and Osher.[15] This dissipation, although necessary in modeling shocks, is undesirable for smooth flows, such as boundary layers. The flux-vector splitters ignore (cannot preserve) contact discontinuities that can be thought of as forming the shear layer but diffuse the linear discontinuities in which there is no intrinsic steepening mechanism counteracting the numerical diffusion. The flux-vector split formulas do not lead to vanishing dissipation in any steady wave, unlike flux difference splitting.[12] In view of these factors, it appears that the numerical dissipation due to splitting in F3D affects the accuracy of the solution and tends to broaden (diffuse) the boundary layer and increase the friction coefficient (see Table 1).

A quantitative description of numerical dissipation present due to Steger-Warming splitting in both ξ and ζ directions for viscous regions with no mass transfer at the wall has been recently reported by MacCormack and Candler[16] along with

Table 1 Comparison of $c_{fx}\sqrt{Re_x}/2$ from exact solution with F3D and boundary-layer codes

C	Exact	F3D	Error, %	Boundary layer	Error, %
−5.0	2.590	2.4281	6.3	2.4782	4.3
−1.5	0.945	0.9362	0.93	0.9026	4.5
−0.5	0.523	0.5464	4.5	0.5059	3.3
0.0	0.332	0.3762	13.3	0.3177	4.3
0.5	0.165	0.2318	40.5	0.1601	3.0
0.75	0.094	0.1745	85.6	0.0897	4.6
1.0	0.036	0.1292	259.0	0.0387	7.4
1.238	0.0	—	—	0.0080	—

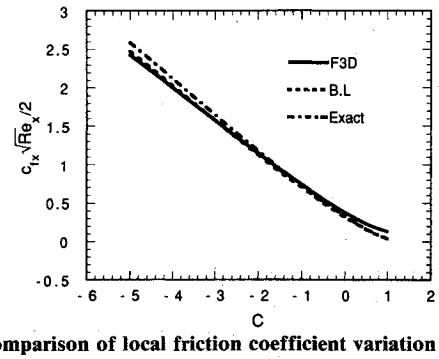

Fig. 6 Comparison of local friction coefficient variation with blowing or suction for laminar flow past a flat plate.

proposed improvements, which are further discussed by van der Vegt.[17] Dissipation errors and improvements in Osher's flux difference splitting[15] and van Leer's flux-vector splitting[12] are presented by Koren.[18] Von Lavante[10] has analyzed dissipation in Roe flux difference splitting.

McCormack and Candler[16] show that in the absence of no blowing at the wall, the numerical dissipation for Steger-Warming flux vector splitting in the normal direction ζ is given by

$$D_{n,\zeta} \propto a(u_{i,k+1} - u_{i,k}), \qquad \text{for } w_b = 0 \tag{8}$$

Because the streamwise velocity gradients in the boundary layer in the normal direction are significant, considerable exchange of tangential momentum between the cells $(i, k+1)$ and (i,k) is numerically produced. It has been shown that large numerical errors occur for laminar flow past a flat plate at $M_\infty = 0.6$ and $Re_x = 4.6 \times 10^6$.

However, in the F3D code the inviscid flux is split only in the ξ direction. By analogy with Eq. (8), the numerical dissipation in this case can be expected to be of the form

$$D_{n,\xi} \propto a(w_{i+1,k} - w_{i,k}), \qquad \text{for } w_b = 0 \tag{9a}$$

Since the normal velocity gradients in the streamwise direction are small in the boundary layer, the numerical dissipation due to flux-vector splitting in the ξ direction given by Eq. (9a) is small. This result is in fact confirmed by the present results for laminar flow described earlier, where for $C = 0$ the numerical results from F3D agree reasonably well with the similarity solution.

The present results for flows with blowing ($C > 0$) suggest a more complicated dependence of the numerical dissipation on the blowing velocity and may be roughly described by

$$D_{n,\xi} \propto af(w_b), \qquad \text{for } w_b > 0 \tag{9b}$$

The solution error due to numerical dissipation increases strongly with an increase in w_b, as demonstrated in Table 1. This dissipation cannot be decreased by decreasing the value of ϵ, since already a very small value of $\epsilon = 0.001$ is employed here, below which the solution becomes independent of ϵ. A detailed assessment and possible control of the numerical dissipation due to flux splitting in F3D in the presence of blowing are beyond the scope of the present work.

Turbulent Flow

Turbulent flow computations at $Re = 10^6$ with uniform blowing past an isothermal wall ($T_w/T_\infty = 1$) are compared with available measurements of skin-friction coefficient for various values of blowing at different Mach numbers. The results are presented as

$$c_{fx}/c_{fx,0} = f(2F/c_{fx,0}) \tag{10}$$

where c_{fx} and $c_{fx,0}$ are, respectively, the local friction coefficients with and without blowing, at the same Re_x (same body station). The data for the ratio are known to be independent of Mach number, Reynolds number, and the ratio of wall temperature to freestream total temperature. As done in laminar flow, the comparisons are made at $x = 0.645$ for the F3D solution and $x = 1.042$ for the boundary-layer solution.

For the F3D solution, the $25 \times 3 \times 61$ grid employed for laminar flow is considered for turbulent flow also. Exponential clustering is employed up to $z = 0.05$, beyond which the grid is stretched at constant ratio of 1.2. The distance of the first grid cell from the wall is fixed at 0.00007. The corresponding value of d^+ is found to be in the range of 1–3, such that the first grid cell lies within the viscous sublayer. This insures proper grid resolution in the wall region. As in the case of laminar flow, the numerical smoothing parameter in the F3D solution is chosen as 0.001. No significant overshoot in the velocity is noted for the turbulent flow prediction by the F3D code, the maximum being of the order of about 1%.

For the boundary-layer code, the $25 \times 3 \times 61$ grid described for laminar flow is considered for turbulent flow also. The value of z_{max} is held in the range of 0.05–0.09. It is generally increased with an increase in F (0–0.01) and Mach number (0.2–2).

In the absence of mass transfer at the wall ($F = 0$), F3D and the boundary-layer code are respectively found to be within 1 and 4% of the friction coefficient from a recommended correlation[8]:

$$c_{fx}/2 = 0.0296\, Re_x^{-0.2} \tag{11}$$

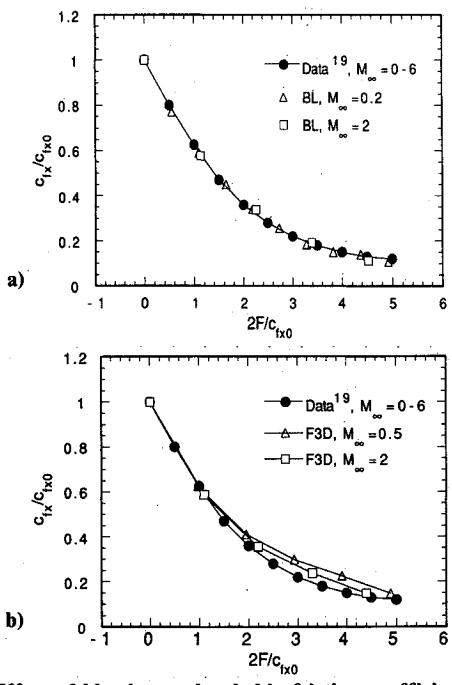

Fig. 7 Effect of blowing on local skin-friction coefficient in turbulent flow over a flat plate at $Re = 10^6$: a) boundary layer code, and b) F3D code.

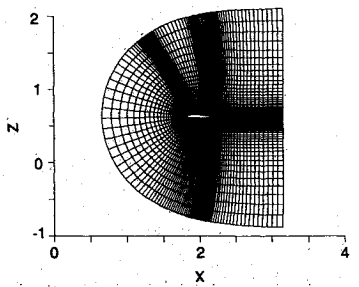

Fig. 8 Two-dimensional grid (139 × 3 × 70) for an airfoil with blowing downstream of leading edge.

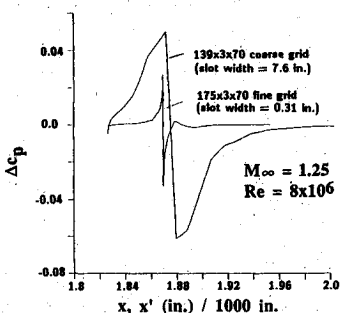

Fig. 9 Effect of slot width on incremental surface pressure distribution due to blowing with discrete mass injection at $M_\infty = 1.25$, $Re = 8 \times 10^6$.

valid in the range of $5 \times 10^5 < Re_x < 10^7$.

The predictions agree well with the measurements[19] over the range of blowing velocities and Mach number considered (Figs. 7a and 7b). Although the boundary layer version yields a friction coefficient ratio, $c_{fx}/c_{fx,0}$, independent of Mach number as indicated by the data, the Navier-Stokes version shows a small dependence of Mach number, especially at large blowing velocities. As the Mach number increases, the predictions become closer to the data. This trend appears to be consistent with the observation that the numerical dissipation inherent in the flux-vector splitting schemes scales with the speed of sound,[12] as demonstrated by MacCormack[16] for Steger-Warming splitting,[5] and by Koren[18] for van Leer's flux splitting scheme.[12]

To study the effect of grid size, F3D solutions for turbulent flow are generated using a $25 \times 3 \times 121$ grid described for laminar flow comparisons. The results from the fine grid are close to those obtained using a $25 \times 3 \times 61$ grid as presented in Fig. 7b, thus confirming the influence of Mach number on the friction coefficient.

Two-Dimensional Flow Past an Airfoil

A two-dimensional airfoil (Fig. 8) with an adiabatic wall using a $175 \times 3 \times 70$ grid is considered to study the effect of blowing at a discrete streamwise station on local surface pressure distribution in turbulent flow at a freestream Reynolds number of 8×10^6 and Mach number of 1.25. The reference lenth L' is taken as 1000 in. Two widely different slot widths (7.6 and 0.31 in.) are considered. The results (Fig. 9) indicate a characteristic rise in surface pressure upstream of injection and a subsequent fall in pressure downstream of injection. The peak values of pressure and the streamwise extent of influence on surface pressure depend on slot width. The downward force upstream of injection is roughly balanced by an upward force downstream of injection. These results are in qualitative agreement with available data.[20]

Conclusion

In laminar flow with and without suction, F3D compares satisfactorily with the exact solution for a flat plate. However, more accurate schemes with lesser numerical dissipation need to be developed for predicting laminar flows with moderate-to-large values of blowing. The slight Mach number dependence in the reduction of the skin-friction coefficient due to blowing, computed by the F3D code, is attributed to the numerical dissipation present in the flux-vector splitting scheme. The computed surface pressures for turbulent flow past an airfoil with mass injection are in qualitative agreement with the data.

Acknowledgments

This work was supported by the Aerosciences Branch of NASA Johnson Space Center under Contract NAS 9-17900. The authors are grateful to the late Joseph L. Steger of the University of California at Davis and to Pieter G. Buning of NASA Ames Research Center for many valuable discussions and suggestions in this effort.

References

[1]Steger, J. L., Ying, S. X., and Schiff, L. B., "A Partially Flux-Split Algorithm for Numerical Simulation of Compressible Inviscid and Viscous Flow," *Proceedings of the Workshop on Computational Fluid Dynamics,* Inst. of Nonlinear Sciences, Univ. of California, Davis, Davis, CA, 1986.

[2]Buning, P. G., Chiu, I. T., Obayashi, Y. M., Rizk, Y. M., and Steger, J.L., "Numerical Simulation of the Integrated Space Shuttle Vehicle in Ascent," AIAA Paper 88-4359, Aug. 1988.

[3]Roth, K. R., "Influence of the Thin-Layer Approximation on Jet in Crossflow Computations," AIAA Paper 90-3056, Aug. 1990.

[4]Beam, R., and Warming, R. F., "An Implicit Finite-Difference Algorithm for Hyperbolic Systems in Conservation Law Form," *Journal of Computational Physics,* Vol. 22, No. 1, 1976, pp. 87–110.

[5]Steger, J. L., and Warming, R. F., "Flux-Vector Splitting of the Inviscid Gasdynamic Equations with Application to Finite Difference Methods," *Journal of Computational Physics,* Vol. 40, No. 2, 1981, pp. 263–293.

[6]Baldwin, B. S., and Lomax, H., "Thin-Layer Approximation and Algebraic Model for Separated Turbulent Flows," AIAA Paper 78-257, Jan. 1978.

[7]Cebeci, T., and Smith, A. M. O., *Analysis of Turbulent Boundary Layers,* Academic, New York, 1974.

[8]Schlichting, H., *Boundary Layer Theory,* 6th ed., McGraw-Hill, New York, 1976, pp. 389–390.

[9]Anderson, D. A., Tannehill, J. C., and Pletcher, R. H., *Computational Fluid Mechanics and Heat Transfer,* McGraw-Hill, New York, 1984, p. 468.

[10]Von Lavante, E., "Accuracy of Upwind Schemes Applied to the Navier-Stokes Equations," *AIAA Journal,* Vol. 28, No. 7, 1990, pp. 1312–1314.

[11]Kays, W. M., *Convective Heat and Mass Transfer,* McGraw-Hill, New York, 1966, pp. 87–89.

[12]Van Leer, B., Thomas, J. L., Roe, P. L., and Newsome, R. W., "A Comparison of Numerical Flux Formulas for the Euler and Navier-Stokes Equations," AIAA Paper 87-1104, 1987.

[13]Van Leer, B., "Flux-Vector Splitting for the Euler Equations," *Lecture Notes in Physics,* Vol. 170, Springer-Verlag, Berlin, 1982, pp. 507–512.

[14]Roe, P. L., "Approximate Riemann Solvers, Parameter Vectors, and Difference Schemes," *Journal of Computational Physics,* Vol. 43, No. 2, Feb. 1981, pp. 357–372.

[15]Osher, S., "Numerical Solution of Singular Perturbation Problems and Hyperbolic Systems of Conservation Laws," *North Holland Mathematical Studies,* Vol. 47, 1981, pp. 179–205.

[16]MacCormack, R. W., and Candler, G. V., "The Solution of the Navier-Stokes Equations Using Gauss-Siedel Line Relaxation," *Computers and Fluids,* Vol. 17, No. 1, 1989, pp. 135–150.

[17]van der Vegt, J. J. W., "Assessment of Flux Vector Splitting for Viscous Compressible Flows," AIAA Paper 91-0243, Jan. 1991.

[18]Koren, B., "Upwind-Discretization of the Steady Navier-Stokes Equations," *International Journal for Numerical Methods in Fluids,* Vol. 11, 1990, pp. 99–117.

[19]Bushnell, D. M., Watson, R. D., and Holley, B. B., "Mach and Reynolds Number Effects on Turbulent Skin Friction Reduction by Injection," *Journal of Spacecraft and Rockets,* Vol. 12, No. 8, 1975, pp. 506–508.

[20]Spaid, F. W., and Zukowski, E. E., "A Study of the Interaction of Gaseous Jets from Transverse Slots with Supersonic External Flows," *AIAA Journal,* Vol. 6, No. 2, 1968, pp. 205–212.

Ernest V. Zoby
Associate Editor